Design and implementation of a bacterial signaling circuit

Lazova, M.D.

2013

document version
Publisher's PDF, also known as Version of record

Chapter 6

Concluding remarks and outlook

We have implemented experiments at the level of signaling and behavior to investigate the design and implementation of one of the simplest signaling circuits in nature: the chemotactic signaling system of enteric bacteria. We demonstrated the fold-change detection property of bacterial chemotaxis, systematically compared the transfer functions of chemotactic signaling and behavioral response in linear gradients of *Escherichia coli* and *Salmonella typhimurium*, and identified and characterized the opposite responses to the cystine / cysteine redox pair of *S. typhimurium*. We explored the function of the phosphorylatable scaffolding protein CheV in *S. typhimurium*, and the phosphorylation-dependent feedback on CheB in *E. coli*. Here we summarize the main findings of this thesis, comment on further questions that have been identified, and discuss experimental approaches and technological developments and that could help answer these questions. We discuss possible future studies based on our findings and potential applications of the research.

Chapter 6

6.1. Fold-change detection in biological sensory systems

Living organisms have evolved sensory systems that allow them to detect changes in their surroundings. Arguably the best-studied bacterial sensory system is the chemotaxis circuit of *E. coli*, which shares common features with other more complex sensory systems. Among these features is the ability to adapt precisely, *i.e.* after a change in the input to a new constant level, the output gradually returns to the pre-stimulus level. Another feature of adaptive sensory systems, well-known in physiology, is that the responses follow Weber's law [247], $\Delta r(s, s_0) = k\Delta s/s_0$, *i.e.* the magnitude of the instantaneous response, Δr, following a small step change in input, Δs, scales proportionately to the ratio of the input change to the background input level, s_0. The proportionality constant k is called the Weber-Fechner constant.

A more general type of adaptive response rescaling that has been recently described theoretically is fold-change detection (FCD) [231]: the entire shape of the response, including its amplitude and duration, depends only on fold-changes in the input and not on its absolute levels, *i.e.* $\Delta r(s(t), s_0) = \Delta r(\gamma s(t), \gamma s_0)$, where γ is constant. In Chapter 2, we provided the first experimental demonstration that FCD holds in a biological sensory system: the chemotaxis circuit of *E. coli* [137] (Figure 6.1). Using *in vivo* FRET and microfluidics respectively, we showed that for the attractant α-methyl-aspartate (MeAsp) the FCD property holds in two adjacent but distinct regimes, both at the level of signaling and behavior. More recently, a study [158] that utilized a noninvasive inference of the chemotactic response function of bacteria by analyzing bacterial trajectories in chemoeffector gradients provided further evidence that the FCD property holds over > 3 orders of magnitude for both MeAsp and glucose.

In Chapter 3, we demonstrated that FCD also holds in the MeAsp response of the closely related species *S. typhimurium*. However, the ranges over which FCD holds, are different between the two species, and we showed that the difference is determined by the sensitivity modulation profile $\psi([L]_0) \equiv \frac{\partial f_t}{\partial \ln[L]}\Big|_{[L]=[L]_0}$ of the kinase response. The interspecies comparison between FCD properties of *E. coli* and *S. typhimurium* could

serve as a starting point for further studies of the evolution of the FCD property in enteric bacteria, as discussed in section 6.2.

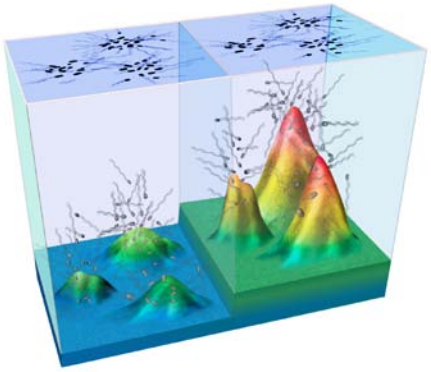

Figure 6.1. Artist representation of bacteria, executing FCD type of chemotaxis response. The nutrient gradients (represented as colored landscapes) are rescaled by the same factor as the background concentration of nutrients, to which the bacteria have been adapted. Image has been created by Gorick G, Bellomo D, Shimizu TS and Stocker R.

Sensory systems could detect multiple types of inputs; in the case of the bacterial chemotaxis system, it can detect multiple chemoeffectors, either by the same or different chemoreceptors (see examples in Table 3.1, Chapter 3). Recently, Uri Alon and colleagues have developed mathematical models to analyze how FCD-type sensory systems respond to multiple input signals [98]. Alon et al. find that if both input signals bind the same receptor independently, the integrated response is multiplicative, *i.e.* the response dynamics depends only on the product of the fold changes in the two inputs.

We can test this prediction experimentally for bacterial chemotaxis by providing cells with two simultaneously varying input signals and using fluorescence resonance energy transfer (FRET) measurements of the type described in Chapter 2. The challenge in this experimental study will be to select a chemoreceptor that can bind independently two chemoeffectors. One candidate is the Tar chemoreceptor of *E. coli* that senses the attractants aspartate, cysteine and maltose, and repellents Co^{2+} and Ni^{+} [170,180]. However, binding of some of these ligands (e.g. aspartate and

cysteine) is not independent [170]. Also some of the ligands (maltose, Ni^{+}) [65,155] are first bound to periplasmic binding proteins, and the formed complexes are detected by the chemoreceptors, which might complicate the analysis of the experimental results. Another strategy to test FCD to multiple simultaneous inputs could be to express in *E. coli* McpS: a heterologous chemoreceptor from *Pseudomonas putida* KT2440, which has two binding sites that has been recently characterized [196]. The membrane-proximal site of McpS binds malate and succinate, whereas its membrane-distal site binds acetate [196]. Heterologous expression of McpS in *E. coli* would provide the possibility to utilize the existing knowledge for the chemotaxis signaling pathway of *E. coli* and characterize the properties of the *P. putida* chemoreceptor. A challenge in these experiments will be to work with acetate, which is a membrane-permeable acid [64] that could perturb the intracellular pH of the cells, affecting bacterial metabolism [37]. Exploring other microorganisms and chemoreceptor types could provide numerous opportunities for studying FCD to single or multiple inputs.

6.2. Quantitative comparative physiology of microorganisms

The molecular composition and topologies of the chemotactic signaling networks demonstrate diversity across bacteria [281]: even between *E. coli* strains, there are differences in the chemoreceptor species composition [133]. In Chapter 3, we performed a FRET-based comparative physiology study of the transfer functions of chemotactic signaling of the two closely related species *E. coli* and *S. typhimurium*. Using FRET measurements with time-varying inputs, we showed that the parameters of receptor and adaptation transfer functions differ between the two species: *S. typhimurium* has three-fold less cooperative response to MeAsp, but the dynamic range of the MeAsp response is ten-fold broader; the adaptation in *S. typhimurium* is three-fold faster. Evaluating the response at different background concentrations of the attractant MeAsp revealed that the sensitivity modulation profile $\psi([L]_0)$, which determines both the drift velocity in steady spatial gradients of attractant and the changes of the kinase activity of chemotactic signaling response differ between the two species (Figures 3.7 and 3.8, Chapter 3).

How the observed differences in the chemotactic signaling and behavior of *S. typhimurium* and *E. coli* will affect the fitness of the bacteria in microniches in which these species coexist? Competition experiments within the same microfluidics platform could provide insights on this question. The two species can be transformed with plasmids that express fluorescent proteins of different colors. Careful selection of spectrally separated fluorescence proteins and optimization of the expression levels will allow distinguishing the bacteria from the two species in a mixed suspension. Bacterial cultures from the two species mixed into defined ratios can be injected in the test channel of a microfluidic device, e.g. of the type shown on Figure 3.7A (Chapter 3) and the distributions of the bacteria can be subsequently recorded using a fluorescence microscopy and high-speed camera. This setup will be useful for distinguishing for subtle differences in behavioral performance that are hard to detect in separate experiments with individual populations. Moreover such competition experiments might allow identification of interspecies interactions affecting the behavioral performance of bacteria.

Recent theoretical studies [114,232] have shown that the drift velocity v_D depends linearly on the gradient of the logarithmic concentration of ligand, $G = d\ln[L]/dx$, before it saturates when G exceeds a critical value G_C (Figure 6.2) [114]. For $G < G_C$, $v_D \approx CG$; the constant $C \propto v^2\tau$, where v is the average run speed and τ is the average run time. G_C is determined by the linear rate constant of receptor methylation K_R ($= F'(a_0)/2$ in the model of reference [260]), rotational Brownian motion, or both [232]. C has been shown to be roughly independent of K_R. The saturating (maximal) drift velocity v_D^{max} at $G \geq G_C$ is also determined by K_R: $v_D^{max} \propto K_R^{1/2}$. The methylation rate for *E. coli* was estimated to be $K_R = 0.005$ s^{-1} [226], and in Chapter 3 we found that *S. typhimurium* adapts three-fold faster, i.e. $K_R = 0.015$ s^{-1}, and the average time to reach steady state of the chemotactic migration coefficient (CMC) [156] is also three-fold shorter in *S. typhimurium*. The dependence of the steady-state v_D on the mean concentration of the gradient $[L]_0$, to which the bacteria were pre-adapted (Figure 3.7, Chapter 3), suggests that the gradients that we used for these experiments are less steep or comparable to G_C for both species (similar to gradient G^I on Figure 6.2). In the future, single-population or competition experiments could be used to explore

different gradients selected such that the steepness is larger than the G_C of one or both species so the maximal drift velocity that the two species can reach depends on their adaptation rates (similar to gradient G^{II} on Figure 6.2). Comparing the behavioral performance under controlled conditions could elucidate the ecological significance of the observed differences in the parameters of chemotactic signaling response and behavior.

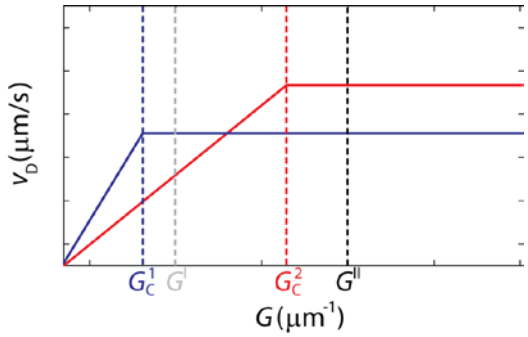

Figure 6.2. Schematic illustration of the dependence of the drift velocity v_D on the gradient of logarithmic concentration of ligand G. Blue and red curves represent two bacterial populations with different values of the critical gradient G_C (G_{C^1} and G_{C^2} respectively). G^I and G^{II} represent hypothetical gradients to which bacteria are exposed (see text).

In Appendix B, we discuss preliminary experiments on the ECOR collection of natural *E. coli* isolates representing much of the current genetic diversity of the species [189,275]. We found that the chemotactic performance in self-created nutrient gradients in soft-agar plates significantly differs between ECOR strains. We identified a subset of strains that have contrasting properties of their chemotactic performance and swimming speed (Table B.2, Appendix B). We have also engineered genetically most of these strains such that they can be used for experiments using our *in vivo* FRET system [242] for measuring the chemotactic signaling response. Future FRET-based comparative physiology studies of the chemotactic signaling transfer functions of the selected ECOR strains, similar to the interspecies comparison that we described in Chapter 3, might allow identification of parameters that are conserved or have diverged in the recent evolution of *E. coli*, and reveal whether different properties of chemotactic signaling such as perfect adaptation, Weber's law or FCD are conserved. Strains in

which one or more of these properties are not conserved could be subjected to further behavioral tests using microfluidics [8], and compared for their fitness (chemotactic performance) under defined gradients.

Figure 6.3 illustrates the first FRET results that we have obtained for an ECOR strain, ECOR51. This strain was selected because it belongs to a phylogenetic group B2, which is distant from group A to which *E. coli* K12 (used as a model strain for the majority of the current studies of chemotaxis) belongs (see Figure B.3, Appendix B). Interestingly, the cooperativity of the response to MeAsp of ECOR51 is three-fold lower than that of *E. coli* K12 (Figure 6.3A). The dissociation constant of the active receptors [260] of ECOR51 appears to be ~10-fold lower than that of *E. coli* K12, however this parameter is not well constrained by our current results; further experiments with higher background concentrations $[L]_0$ would be necessary to confirm this conclusion (Figure 6.3A). The frequency response of ECOR51 at $[L]_0 = 0.229$ mM MeAsp, however, is identical to that of *E. coli* K12 (Figure 6.3B), suggesting that the system-level adaptation properties of the two strains are the same (see Chapter 3).

We have also found that the sensitivity modulation profile $\psi([L]_0)$ of ECOR51 to exponential sinewave inputs has a shape of a single broad peak (see Figure 6.3C), indicating the existence of a single FCD regime in this strain over the range $[L]_0 = (0.018\text{-}0.229)$ mM MeAsp. The main MeAsp receptor, Tar, of ECOR51 has only two residues different from that of wild type *E. coli* K12: Y131H and A184V, both in the cytoplasmic region [189]. The different shape of the sensitivity modulation profile of ECOR51 suggests that it is likely that the properties of its chemoreceptor population differ from that of wild type *E. coli.*

Further experiments of this type with this and other ECOR strains could start a comparative physiology study that would provide an opportunity to study the design principles involved in evolutionary optimization of chemotaxis system, generating phenotypic variability while preserving the important functional features of this system.

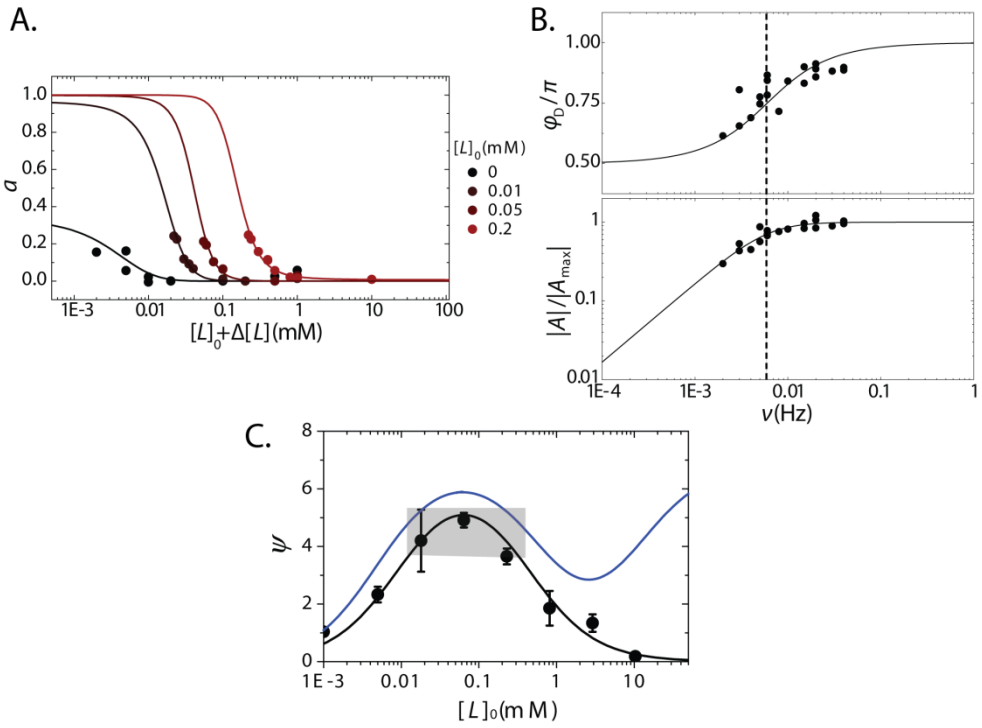

Figure 6.3. Kinase response of ECOR51. **(A)** Dose-response data of the kinase activity (a) to steps of MeAsp, applied to ECOR51 cells, adapted at different background concentrations of MeAsp, $[L]_0$. Fits using the MWC model [260] are shown with parameters $N = 2$, $K_I = 0.018$ mM and $K_A = 0.239$ mM. **(B)** Bode plot for ECOR51, showing the phase delay (top) and the normalized amplitudes (bottom) of the output sinusoids as a function of the driving frequency ν (see Chapter 3). The characteristic frequency for ECOR51 chemotactic signaling response ($\nu_m = 0.006$ Hz) is indicated with a dashed line. **(C)** Sensitivity modulation profile $\psi([L]_0)$ for ECOR51 in response to inputs of the type shown on Figure 3.8A (the fitted parameters are $N = 7$, $K_I = 0.01$ mM and $K_A = 0.4$ mM, see Chapter 3). $\psi([L]_0)$ for wild type *E. coli* (blue) is shown for comparison (see Chapter 3). The plateau of invariant responses of ECOR51 is indicated by the shaded rectangle. Error bars represent standard deviation from 2-5 repeats.

6.3. Opposite responses to a redox pair

We discovered a redox pair, cystine / cysteine, which elicited chemotactic signaling responses of opposite signs in *S. typhimurium.* The reduced form, cysteine, is sensed as an attractant, and the response is Tsr / Tar-dependent [138] (Chapter 4, Appendix A). The oxidized form, cystine, elicits a repellent response over a broad concentration range (20 nM – 500 μM), and the amplitude of the response scales linearly with the logarithm of cystine concentration over more than four orders of magnitude, which is not typical for a response that is based on receptor-ligand interactions (Appendix A). In Chapter 4, we showed that deletion of *mcpB* and *mcpC* genes in *S. typhimurium* 14028 abolishes the repellent response to cystine, indicating that McpB and McpC are involved in cystine sensing [138]. However, Δ*mcpB* Δ*mcpC S. typhimurium* LT2 is able to sense cystine even at nanomolar concentrations, suggesting that in this strain there is also an McpB / C-independent pathway of cystine response. The strain-based differences of *S. typhimurium'*s response to cystine could be a subject of further investigations.

Based on the similarity of the time series and the dose-dependent response to cystine and another oxidized compound, benzoquinone, as well as the observation that the response to cystine-cysteine mixtures can have either a positive or a negative sign, depending on the redox potential of the mixtures, we hypothesized that the chemotaxis responses to cystine / cysteine pair are likely to be mediated by a redox-dependent pathway (Appendix A). Cystine / cysteine redox gradients are likely to be formed in nature in the presence of oxidizing agents [142]. Oxidative environments generate reactive oxygen species, which are responsible for damage to all macromolecules (DNA, lipids and proteins) [205]. Thus, redox-sensing mechanisms that allow the bacteria to sense and avoid oxidative conditions might facilitate *S. typhimurium* survival.

We sought to understand how the observed modes for cystine and cysteine sensing aid *S. typhimurium* to orient in gradients, formed by cystine / cysteine redox pair. We performed pilot experiments using the microfluidics platform [7], described in Chapter 3 (see Figure 3.7A). By injecting cystine / cysteine in the flanking channels of the platform (source

and sink channels), we created spatial gradients of cystine and cysteine. Using a video microscopy, we recorded the time evolution of the distribution of *S. typhimurium* populations within the test channel. To estimate the strength of the chemotactic response, we computed the chemotaxis migration coefficient (CMC), which represents the mean displacement of the population from the center of the test channel [156], *i.e.* $CMC(t) \equiv (\langle x \rangle(t) - W/2)/(W/2)$, where W is the width of the test channel, and $\langle x \rangle(t)$ is the mean position of the bacterial population along the gradient. Negative *CMC* indicates a displacement of the population towards the sink channel, and positive *CMC*: displacement of the population towards the source channel.

Although bacteria accumulate towards increasing concentrations of cysteine in cysteine gradients, as expected from the attractant response observed in the FRET experiments, no response is observed for populations of *S. typhimurium* placed in a gradient of cystine (Figure 6.4A). However, when the cysteine and cystine were mixed together and used to create a gradient by injecting the mixture in the source channel and flowing only motility buffer through the sink channel, *S. typhimurium* populations moved in opposite directions depending on the cystine / cysteine ratio. When we injected a mixture of 10 mM cysteine and 0.5 mM cystine in the source channel, the bacteria moved towards the source, *i.e*. showed an attractant response to the mixture (Figure 6.4B). On the contrary, when we injected a mixture of 10 mM cysteine and 1 mM cystine in the source channel, the bacteria moved away from the source channel, *i.e.* showed a repellent response to the mixture (Figure 6.4B). Moreover, if we inject cysteine and cystine in the opposing flanking channels (source and sink respectively), the attractant response is stronger than that elicited by a gradient formed by the same concentration of cysteine in the source channel versus a motility buffer only in the sink channel (Figure 6.4).

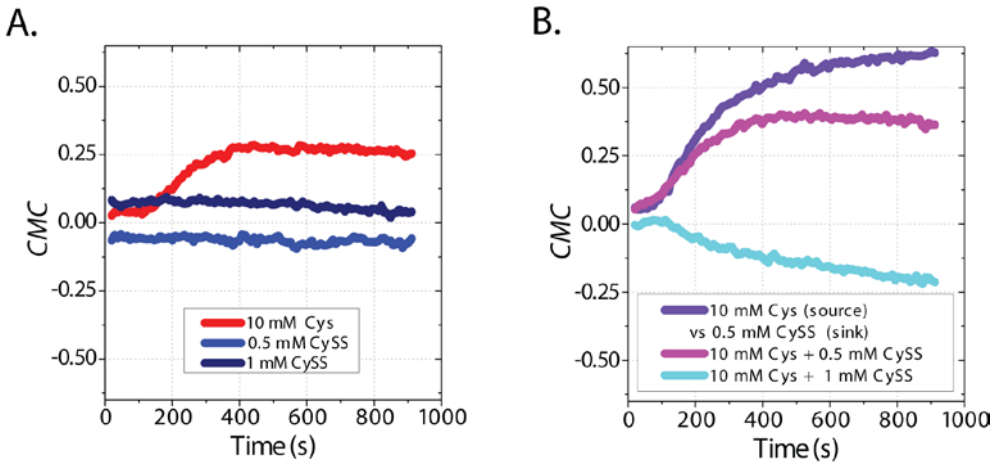

Figure 6.4. Response of *S. typhimurium* LT2 to spatial gradients of the cystine / cysteine redox pair. Steady linear gradients were created in microfluidic platforms with parallel source, test and sink channels (see Figure 3.7A). **(A)** 10 mM cysteine, 0.5 mM cystine or 1 mM cystine was injected in the source channel. Only motility buffer was flown through the test channel. For each of the three gradients, *CMC* of wild type *S. typhimurium*, injected in the test channel, is shown. **(B)** Mixtures of 10 mM cysteine and 0.5 mM or 1 mM cystine were injected in the source channel, whereas only motility buffer was flown through the test channel. The third gradient (purple) was created by flowing 10 mM cysteine in the test channel and 0.5 mM cystine in the sink channel. For each of the three gradients, *CMC* of wild type *S. typhimurium*, injected in the test channel, is shown.

These preliminary experiments with cystine / cysteine spatial gradients demonstrate that these compounds invoke a motile chemotactic response under certain conditions. Whether this response is dominated by the redox conditions or cysteine concentration, the reason for the lack of response to cystine-only gradients, and how cystine affects the response to cysteine gradients could be a subject of further investigations. Further experiments probing the response of receptor-mutant *S. typhimurium* strains in cystine / cysteine gradients could also be used to address the contribution of the individual receptors to the cystine / cysteine response.

Cystine / cysteine responses could be relevant for survival and spreading of the pathogen *S. typhimurium* in the host. Although little is

known about the habitat of the enteric bacteria in the gut, it is unlikely that steady amino acid / redox gradients are formed in the lumen. However, close to the wall of the intestine, there is a mucus layer, consisting of glycoprotein (mucin), proteins, carbohydrates and lipids [59,253]. The composition and rapid turnover of the mucus suggests the formation of amino acid / peptide gradients. The role of the mucus layer in protecting the underlying epithelial cells from contact with the luminal gut bacteria is largely unknown [60].

We hypothesize that chemotaxis response to cystine / cysteine might guide bacteria through the mucus layer towards the epithelial layer, facilitating systemic infections. Some of the mucins are cysteine rich, and cysteines get crosslinked by disulfide bridges, giving the gel structure of the mucus layer, which prevents bacteria from entering the layer [125]. Defects in the crosslinking of the mucus, e.g created by locally reducing conditions, might provide a path for systemic invasion of the bacteria. The opposite responses to the cystine / cysteine redox pair might improve the ability of the pathogenic *S. typhimurium* strains to find such crosslinking defects in the structure of the mucus layer, and facilitate systemic infections [145].

6.4. Phosphorylation-dependent feedbacks in bacterial chemotaxis

The activity of the methylesterase enzyme CheB of *E. coli* is feedback-regulated via phosphorylation by the kinase CheA on its regulatory (REC) domain: the phosphorylation induces a conformational change in the REC domain, which activates the methylesterase activity of CheB [69], which in turn enhances the deactivation of the receptor-kinase complexes [15]. In Appendix C, we probed whether the sharp transition of the methylation-dependent feedback transfer function $F(a)$ at high values of a is a consequence of the phosphorylation feedback on CheB activity. We used *E. coli* mutants that cannot be phosphorylated because the REC domain of CheB is knocked out or the phosphorylation site of CheB is disrupted. The shape of $F(a)$ in the mutant strains, lacking the REC domain and having a steady-state kinase activity >0.40, followed Michaelis-Menten kinetics, suggesting that the phospho-regulation of CheB activity might cause the sharp decrease of $F(a)$ in wild type cells (Figure C.2, Appendix C).

Another phosphorylation-dependent feedback might exist in the chemotaxis system of *S. typhimurium*, which has a scaffolding protein CheV that contains a REC domain [10]. Our experiments with methylation deficient *S. typhimurium* suggested that a partial methylation-dependent adaptation to MeAsp exist in CheV+ but not in CheV- cells (Chapter 5), and this adaptation might be phosphorylation-dependent: CheV mutant with genetically disrupted phosphorylation site does not complement the defect of Δ*cheV* methylation-deficient cells. Furthermore, using a fluorescent marker for the chemoreceptor clusters (YFP-CheR) we revealed that the number of lateral clusters decreases in CheV- cells, suggesting that CheV plays role in chemoreceptor clustering (Chapter 4).

The role of CheV in *S. typhimurium* chemoreceptor clustering and adaptation could be investigated in future studies of bacteria with altered chemoreceptor species composition. These studies might reveal that only part of the chemoreceptor species in *S. typhimurium* are coupled to the kinase via CheV. Identification of chemoreceptors, which couple to CheA in CheV-dependent manner will facilitate further physiological studies of CheV function, using chemoeffectors that are sensed specifically by these chemoreceptors.

6.5. Acknowledgements

The microfluidics experiments with cystine / cysteine were performed in the lab of Prof. Dr. Roman Stocker (Massachussetts Institute of Technology).

Chapter 6